



# Modeling of 3D woven composites using the digital element approach for accurate prediction of kinking under compressive loads



Shreyas Joglekar (Graduate Research Assistant), Mark Pankow (Assistant Professor)\*

Department of Mechanical and Aerospace Engineering, North Carolina State University, Raleigh, NC 27695, USA

## ARTICLE INFO

### Article history:

Received 13 October 2016

Accepted 18 October 2016

Available online 19 October 2016

### Keywords:

3D woven composites

Kink band formation

Realistic geometry modeling

## ABSTRACT

Model definition accuracy dictates the reliability of a predictive analysis for 3D woven composites (3DWC). The traditional modeling approach is based on analysis of ideal geometry with user specified imperfections. In that case, co-relating the actual imperfections arising from manufacturing processes with that of the model becomes an iterative process. In this study, a digital element (DE) approach is implemented for creating the woven architecture of the composite. This technique simulates the individual fibers and their interactions allowing the user to create a reference unit cell with imperfect geometry induced during manufacturing stages of 3DWCs. Thus the response and strength analysis account for the unique weaving signature and provide better predictions without the necessity to run iterative analysis procedures required for idealized geometry models. X-ray CT images or detailed statistical data for variations in specimen geometry are not required which makes this approach more attractive in terms of cost and creation time. A representative model created using the DE approach is used for prediction of compressive failure of 3DWC without having to seed imperfections for failure initiation. The analysis also captures the formation of a kink band as observed in experimental tests. Results of this study are compared with the experimental results and simulation results of idealized geometry reported previously in literature.

© 2016 Elsevier Ltd. All rights reserved.

## 1. Introduction

3D woven composites (3DWC) are extensively used in aerospace applications because of their better resistance against impact and delamination in comparison to laminated composites. 3DWCs have an additional binding fiber tow (or Z-fiber tow) running through the thickness, that results in enhanced impact and delamination resistance properties. However, due to waviness of the Z-fiber tow, imperfections are introduced in the warp and weft tows in the vicinity of Z-fiber tows during the manufacturing. Such defects significantly affect the response and strength characteristics. Studies on the compressive behavior of 3D composites indicated that kink band formation is the primary mode of failure and it is highly influenced by the geometric flaws in the woven structure [1]. An analytic expression for buckling of a delaminated 3DWC was reported in [2] with the assumptions of no defects and idealized geometry. In practice, the actual response was noted to be much lower due to distortions in the fiber tows. Thus, accurate

modeling of the complex woven geometry with imperfections is the key in predictive analysis. Fleck et al. [3] successfully correlated a cohesive zone model of failure of notched 2D laminates into 3DWC and verified that micro buckling of fiber tows is the dominant failure mechanism. The influence of imperfections was also verified experimentally. Cox et al. [4] carried out a series of experiments and established failure mechanisms for various loading conditions. Experiments by Stig et al. [5] suggested that the imperfections can also initiate crimp mode of failure.

Finite element (FE) simulation accuracy is always limited due to the discrepancy between actual fiber tow geometry of the specimen and the simplified geometric model [6,7]. Models for a 3DWC are generally based on experimental observations or an analytic approach. Every 3DWC can be characterized by its unique weaving arrangement of different types of tows. This pattern of arrangement which is repeated throughout the 3DWC is represented by the smallest possible number of tows called repetitive unit cell (RUC). Commonly used modeling techniques rely on making representative geometry, which simplifies the architecture and often eliminates complicated geometry features that are associated with failure [8,9]. These cells also require samples to be manufactured and measured to determine the actual geometry.

\* Corresponding author.

E-mail addresses: [sjoglek@ncsu.edu](mailto:sjoglek@ncsu.edu) (S. Joglekar), [mrankow@ncsu.edu](mailto:mrankow@ncsu.edu) (M. Pankow).

Measurements are often made through the use of images obtained from an X-ray CT scan or microscope images taken from slicing through a sample. These images show that during the weaving process, the warp (longitudinal) and weft (transverse) tows along with Z-Fiber tows interact with each other resulting in unique geometry [10,11]. This cannot be captured through simplified geometry, which eliminates the imperfections of the actual woven material. Additionally, a particular image provides details of only that particular section of the specimen. To fully understand the complex interactions of fiber tows, it is necessary to consider the overall geometry of the composite with several types of deviations arising from various imperfections and interactions. Yushanov and Bogdanovich [12] implemented a stochastic approach to consider the deviations in the mean fiber tow path. Using parametric equations and user defined deviation functions, an imperfect path can be obtained and represented. This approach of user defined imperfections can be implemented using the commercially available software WiseTex™ [13] and TexGen™ [14]. A comprehensive and realistic model building approach was proposed by Vanerschot et al. [15] which involves a statistical analysis that considers variability in fiber tow paths as well as their average trends and deviations. The approach also implements data from X-ray CT scans for the creation of realistic geometry.

Although these advanced approaches address the imperfections in the fiber tow architecture, implementation of these defects is completely user defined and controlled. To effectively understand their influence on the final properties, it is necessary that these imperfections be adequately distributed throughout the RUC in terms of their location, nature and amplitude. This demands a large number of input parameters and X-ray CT images with thorough analysis to draw effective correlations as presented in [15]. With the objective of combining the simplicity of an idealized geometry model and the accuracy of a realistic approach, the RUC is modeled using a digital element approach proposed by Wang et al. [16]. During the manufacturing processes, fiber tows are subjected to various loads such as tension, compression and friction between each other. These forces cause changes in localized orientations and curvatures. These localizations are important as strength properties of composites are strongly dictated by these geometric details.

The DE approach can accurately capture these effects without a significant addition to processing time. A similar approach of digital elements was implemented using LS-DYNA™ and TexGen™ for model creation [11]. X-ray CT scans showed good correlation of model geometry with the actual specimen [11]. Further, the model was shown to be capable of predicting tensile strength with high accuracy [17]. Geometric models created using the DE approach in DEA Fabric Mechanics Analyzer™ (DFMA) show very good correlation with X-ray CT images of manufactured specimens [10,18]. Geometric models created using DFMA™ accurately predicted the elastic stiffness properties [19].

In this work, the DE approach using DFMA™ is used to create unique geometry that is then imported into FE software. The computational models are then used to predict the compressive response including the buckling behavior of a 3DWC. These new simulations are compared to an idealized geometry model and to experimental data. The model using the DE approach will enable researchers to accurately predict material response without having to fabricate the material.

## 2. Specimen properties

The material used in this study is a 6% Z-fiber tow reinforced 3D woven composite. This composite uses S2 glass fiber tows and SC-15 epoxy, a thermoset polymer, for the matrix material. The elastic

modulus and Poisson ratio for the matrix are 2.48 GPa and 0.36, respectively [20], and for S2 glass fiber tow are 114.2 GPa and 0.22, respectively [21]. Using fiber volume fractions for warp and weft tows reported previously [20] and the material properties mentioned above, elastic properties of constituents of a RUC can be calculated [22,8] as reported in Table 1.

The stress–strain response of fiber tows in the transverse direction can be determined by analyzing a finite element model based on fiber volume fractions shown in Fig. 1 [23]. Fig. 2 shows the nonlinear stress–strain response results from experimental testing of pure matrix material [8] and the stress–strain response of the fiber tow from computational results. The stress–strain response in the axial direction is well known to be dominantly elastic with very small amount of plastic deformation. Due to lack of well-defined yield point in axial direction, the yield ratio is varied from 7 to 20 to observe the corresponding effects of varying degree of plasticity [24].

## 3. Computational model

The RUC models in this work are constructed using Fabric Mechanics DFMA™ software. This section will use an example based on a specimen previously presented [8] to provide a basic overview of the technique and a detailed description of how a model can be made. Fig. 3 compares the images of the architecture from a micro CT scan with the idealized geometry work [8] previously reported and those predicted with the current proposed method.

Fig. 3(c) clearly shows that the proposed method does not assume ideal geometry with perfectly straight tows and cross sections with uniform area as seen in Fig. 3(b). This difference is discussed in more detail in upcoming sections. Fig. 4 shows an overlap comparison of the DFMA™ model with scans of the manufactured specimen. This comparison shows that the model accurately captures the deviations and imperfections in the actual specimen that were created by manufacturing processes.

As shown in Fig. 5, each fiber is represented by a chain of digital rod elements connected by frictionless pins. If the length of the elements approaches zero, the digital chain becomes fully flexible. The rod elements are assumed to have a circular cross section. If the distance between the two yarns becomes less than the diameter of an individual yarn, a contact element is established between these two yarns at the common node. A contact element is a two node element with three degrees of translation freedom per node. Thus, it allows compression along the contact line (local X direction) and friction in the two mutually perpendicular axes (local Y and Z direction). Assembly of multiple digital chains with contact elements then accurately captures the flexibility of fiber tows. The extent of flexibility is governed by the length of rod elements and hence the size of digital elements is much smaller than typical finite elements. Digital rod elements do not necessarily exhibit the properties of the body they represent (fiber tow in this case). For

**Table 1**  
Calculated elastic properties of a RUC.

	Warp (GPa)	Weft (GPa)	Z-Fiber Tow (GPa)
E11	62.83	66.59	64.84
E22	7.24	7.67	7.59
E33	7.24	7.67	7.59
$\nu_{12}$	0.219	0.219	0.22
$\nu_{13}$	0.219	0.219	0.22
$\nu_{23}$	0.272	0.272	0.27
G12	3.28	3.48	3.45
G13	3.28	3.48	3.45
G23	2.84	3.01	2.99

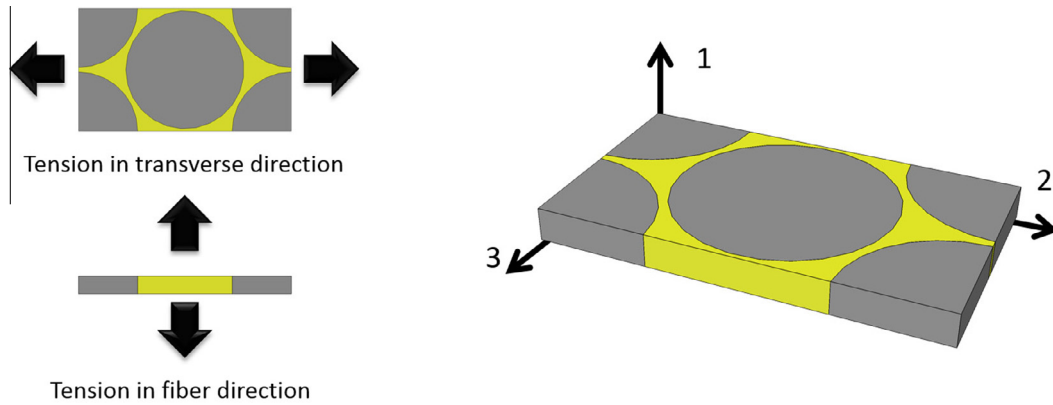


Fig. 1. Volume fraction based fiber tow-matrix finite element model [23].

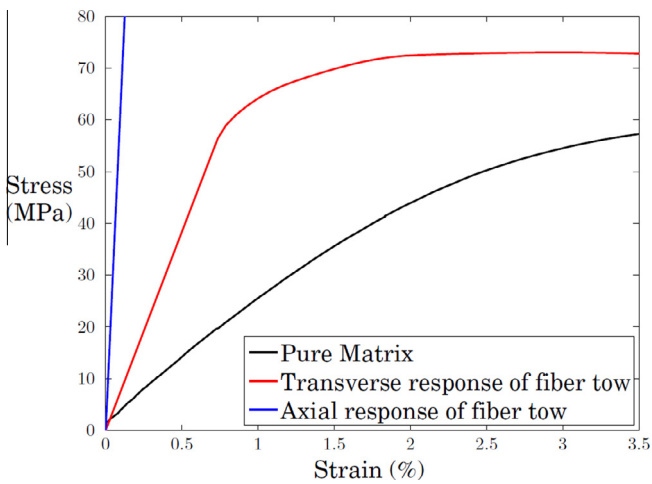


Fig. 2. Plastic response of matrix and fiber tows [8].

example, the flexible nature of yarns is captured by the link of rod elements and not individual rod elements. This highlights the difference between digital elements and conventional finite elements. The details of the approach are explained by Wang and Sun [16]. The model creation approach is summarized by the flow chart in Fig. 6. In this figure, rectangular blocks indicate input or output stages and parallelogram indicates computational processing stage.

### 3.1. Geometric input parameters

The geometric input parameters include visual properties such as cross sectional area and the arrangement of fiber tows. Please refer to Appendix A for details.

#### 3.1.1. Cross sectional area

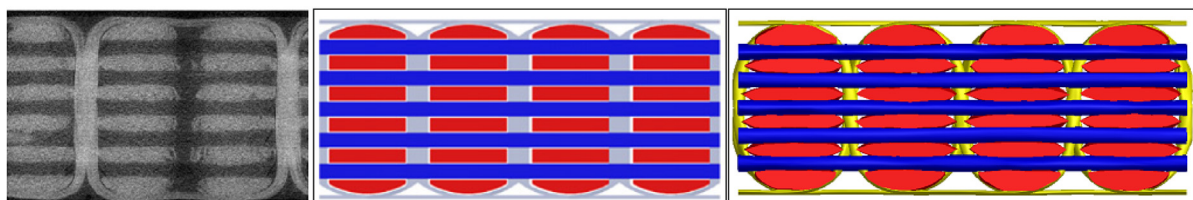
Each type of fiber tow can be assigned an effective cross sectional area representing different sized tows. The effective cross sectional areas for all the 3 types of fiber tows – warp (X direction), weft (Y direction), and Z-fiber tows (binding fiber tows propagating in x direction) are defined. These values can be based on either experimental observations or inputs from the effective size of a fiber tow from the setup on the loom.

#### 3.1.2. Topology

The topology parameters define the arrangement of different types of tows relative to each other. The cell length and width determine the in plane bounds for the cell geometry. For reference, average dimensions at the edge of RUC are reported in Table 2. These values represent final values after multiple iterations involving scaling in X, Y and Z directions. To avoid the interpenetration of the tows, the initial value of width and length should be slightly higher than the final configuration. After defining the bounds of the RUC, the arrangement of tows can be defined accurately and unambiguously using the parameters as shown in Fig. 7.

In an idealized geometry model, the cross section shape (circular, rectangular or elliptical) is assumed to be consistent throughout the length of the tow. In the DE approach, the initial cross section is assumed to be circular but the iterative procedure results in irregular ellipse type geometry that varies as a function of the length. The transition can be seen in Fig. 8. This slight deviation in the cross sectional area is because of effect of surrounding fiber tows.

In addition to these parameters, each warp section needs to be defined accurately for number of warps and Z-fiber tows along with their arrangement in tabular form. For example, the number of tows in section 1 is 5 (only x direction warps) while that for section 2 is 1 (only Z-fiber tows). Table 3 shows tabular arrangement to define position of warp and Z-fiber tows. Only 2 tables are shown for comparison. In practice, they need to be defined for each and every warp section. Wefts, warps and Z-fiber tows are denoted



a) Images from CT scan [8]      b) Ideal geometry [8]      c) Proposed geometry

Fig. 3. Comparison of the computational models with actual images. (a) Images from CT scan [8]. (b) Ideal geometry [8]. (c) Proposed geometry.

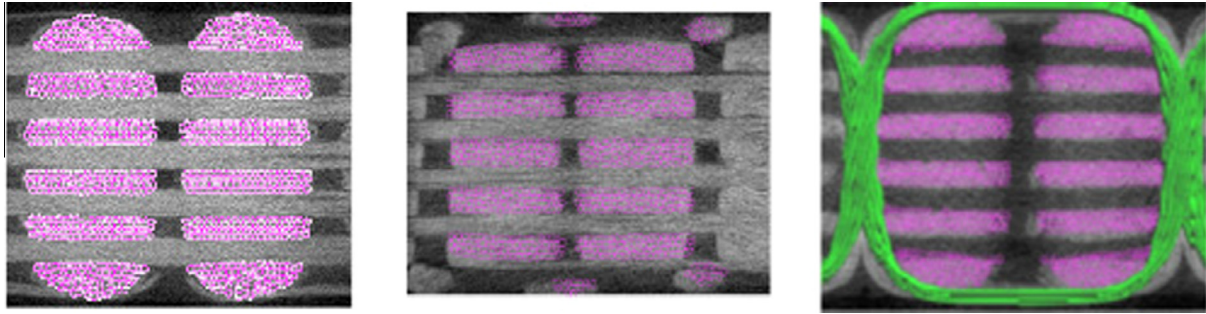


Fig. 4. Comparison of a model created using DFMA™ with X-ray CT scans [26].

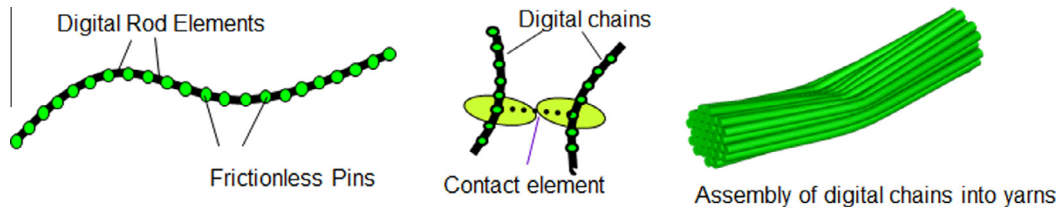


Fig. 5. Building blocks of the model using the digital element approach [25].

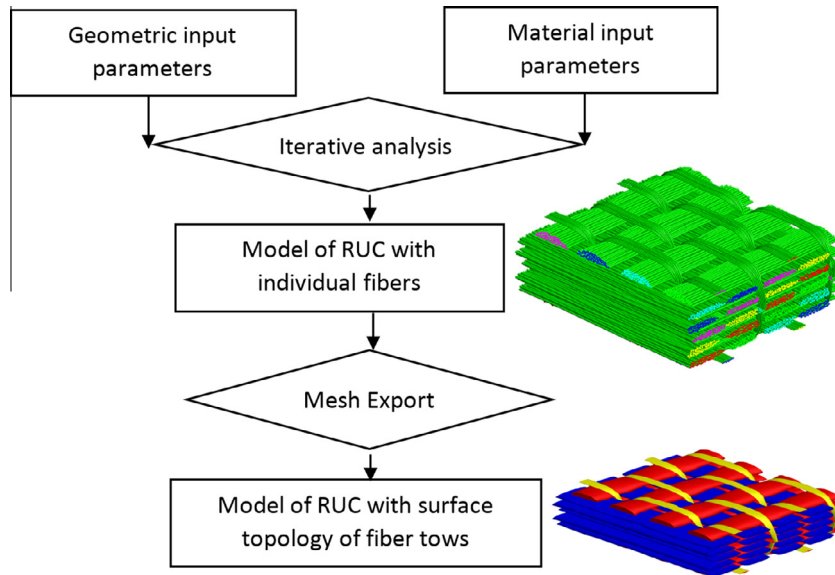


Fig. 6. Creation of geometric model using digital element approach.

**Table 2**  
Unit cell dimensions for model geometry.

	Width (mm)	Length (mm)	Thickness (mm)
RUC	6.83	8.16	6.72
Warp	2.98	8.16	0.48
Weft	3.27	6.83	0.52

by type 1, 2 and 3 respectively. Number of rows and columns in the tables is equal to number of tows per section and number of weft columns respectively as defined earlier. Please refer to [Appendix A](#) for details.

### 3.2. Material input parameters

The material input properties consist of the modulus, strength, density and approximate number of fibers per tow for each tow type. However, as explained by Wang [16], these properties do not necessarily represent actual stiffness properties. It is preferable to start the iterations with actual stiffness properties. But these values can be adjusted by 2–3 orders of magnitude to get desired compliance in the tows so that the RUC can achieve higher volume fractions. This procedure requires manual examination of tow shapes after each iteration which will dictate the choice of parameter values in next iteration.

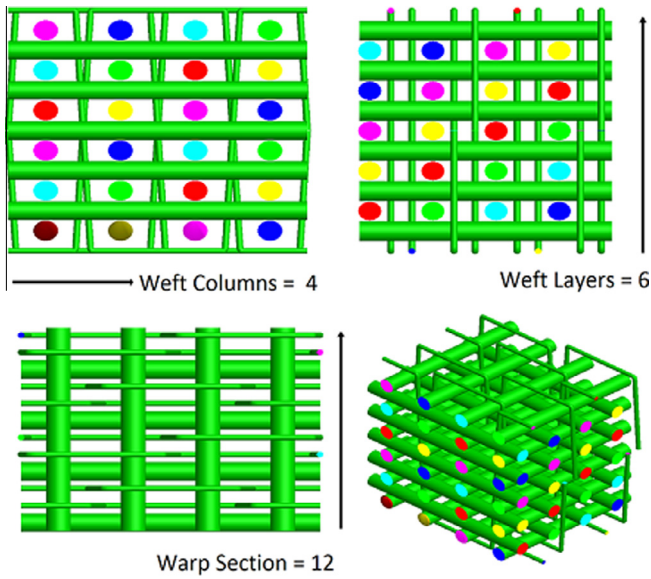


Fig. 7. Geometric parameters for construction of RUC.

3.3. Iterative analysis

After the topology is successfully defined, the objective is to increase the volume fraction of the cell by reducing the thickness while controlling the yarn tension, boundary conditions and some additional computational parameters. Fig. 8 shows evolution of the unit cell model from the simplified initial geometry. The final model used in this analysis was achieved in 6 iterations. In each iteration, more fibers are added to the tow so that the assembly of multiple fibers can accurately represent the unique imperfections in different tows. Average time for each iteration was approximately 6 min on 4 cores with 8 GB RAM. The computational time

is highly dependent on the iteration step parameters. Please refer to Appendix A for details.

3.4. Mesh export parameters

The final geometry created by DFMA™ is exported in .stp format for finite element analysis. The export parameters can be adjusted to accurately capture the tow bending and geometric imperfections. Smaller element size is desirable for accuracy and to avoid fiber tow penetration. The effect of export parameters of Fabric Mechanics DFMA™ is shown in Fig. 9. Before the geometry is ready for analysis, it is important to check for and eliminate yarn interpenetration. When interpenetration occurs, a small region of the geometry is shared by more than one tow resulting in irregular surfaces as shown in Fig. 10. Generally, such regions occupy a small irregular volume which poses problems in defining the mesh and in assigning material properties and orientations. An irregular mesh in these regions causes stress concentration resulting in excessive deformations which ultimately leads to erroneous results.

The interpenetration may take place during the iterative procedure to achieve desired volume fraction. This can be avoided by adjusting the ‘gap factor between yarns’ which is a relaxation parameter of DFMA™. Most of the time, interpenetration will occur in the thickness direction during the compaction of RUC (Z-fiber tows interacting with the other tows). This can be avoided by creating a thicker initial RUC model which seeds enough gap between the tows to prevent interpenetration. The final model is then scaled back to the desired dimensions. However, this will result in reduced fiber volume fraction of the model geometry.

Additional penetration problems can be solved when exporting the geometry into the FE software. This can be controlled by ‘yarn model parameters’ of DFMA™. Generally Z-Fiber tows need much finer export parameters as shown in Fig. 9 compared to warp and weft tows. Highly refined models will have a large number of elements which necessitates finer export control parameters to maintain accurate geometry.

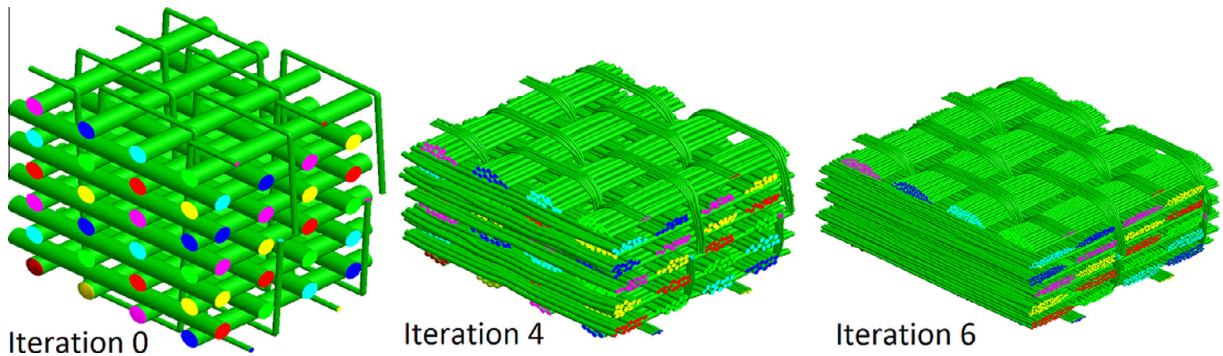


Fig. 8. Development of model using DE approach.

Table 3  
Definition of warp sections.

	1	2	3	4	Yarn Type
<i>Warp section 1</i>					
#1	1	1	1	1	2
#2	2	2	2	2	2
#3	3	3	3	3	2
#4	4	4	4	4	2
#5	5	5	5	5	2
<i>Warp section 2</i>					
#1	6	0	0	6	3

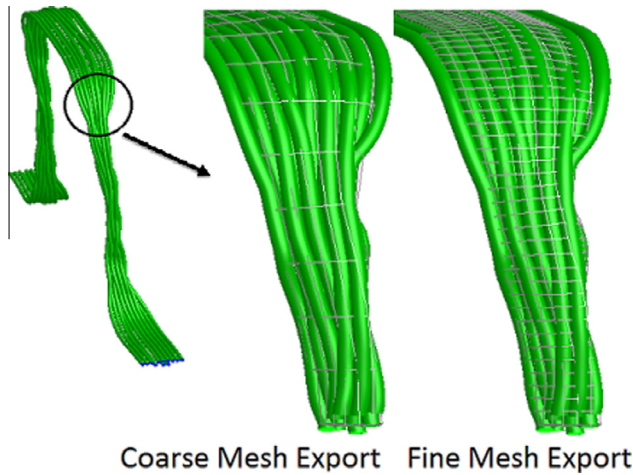


Fig. 9. Effect of mesh export parameter on fiber geometry.

### 3.5. Finite element analysis

To have a complete model of a composite RUC, the fiber tow geometry must be surrounded by matrix in all directions. A hollow block as shown in Fig. 11 replicates all the imperfections in the tows and thus can be treated as the matrix.

Table 4 compares the fiber volume fraction of model RUC against experimental specimen and ideal geometry model reported earlier. The RUC may not always have an integer number of warps. For example, as shown in Fig. 11, the edges of RUC have only half of the warp cross section. To achieve such partial sections, an array of multiple RUCs needs to be created. Then the desired sized RUC can be created by cutting along the length and width.

The final dimensions of the model RUC are within 5% of experimental measurements. The commercial software ABAQUS™ is used for mesh generation and stress analysis. The minimum number of elements is dictated by the export parameters used in DFMA™ software but higher mesh density can be defined for a particular region if required. The entire part is meshed using 4 node linear tetrahedral element (C3D4) of ABAQUS™. Typical element size in Z-Fiber tows is approximately 5 times smaller than that of warps and wefts. The total number of elements is approximately 340,000. Isotropic material orientation has been assigned to all of the elements belonging to the matrix. The fiber tows' orientations change constantly along their length which must be accounted for. Local orientations are assigned to the elements based on 3 or more curved paths defined from individual tows from the DFMA™ software. These are chosen to represent the primary axis (material direction 1) of the Z-Fiber tow for different spatial locations. Fig. 12 summarizes the procedure of assigning material orientation. (The red and black arrows in Fig. 12 are for representation only. In actual model, orientations are calculated for every element differently.)

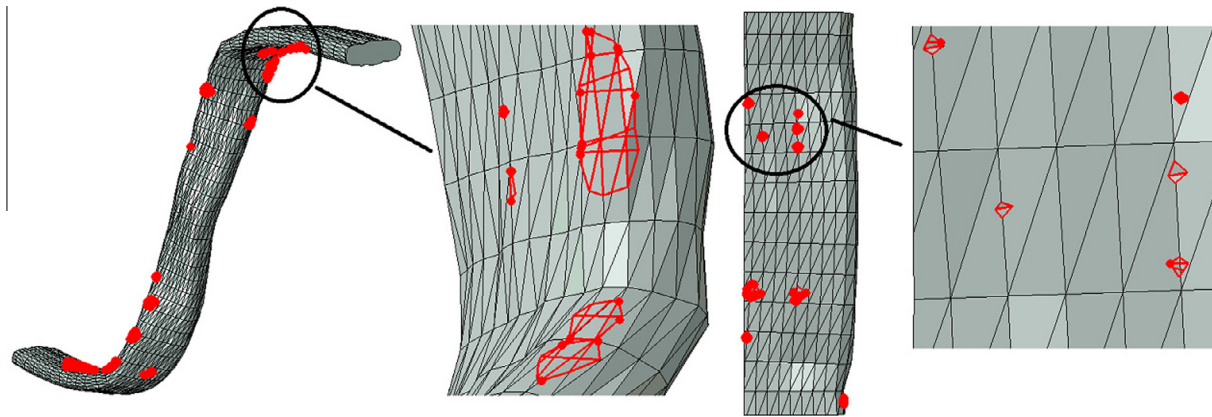


Fig. 10. Irregular geometry resulting from tow penetration in z-fiber and warp tow.

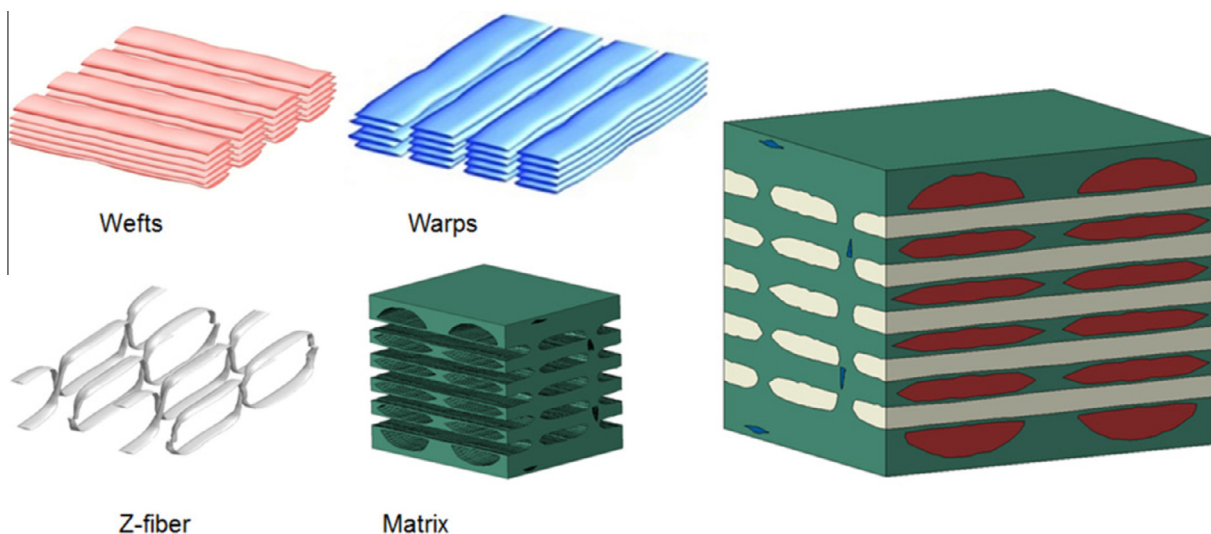


Fig. 11. Single RUC with the components.

**Table 4**  
Comparison of volume fractions.

	% Volume fraction				V(Voids)
	Vf (warp)	Vf (weft)	Vf (z-fiber)	Vm	
Ideal Geometry model [20]	19.07	20.96	1.97	58	0
Manufactured [20]	20.66	22.03	3.21	53.5	0.6
DE Geometry model	26.24	29.77	0.83	43.16	0

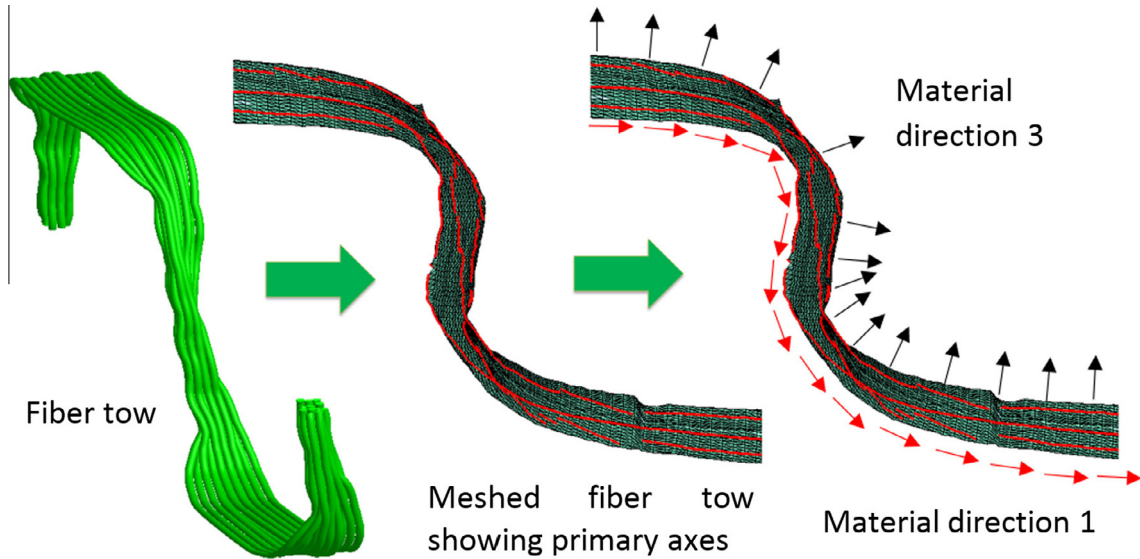


Fig. 12. Assigning the material orientation for z-fiber tows.

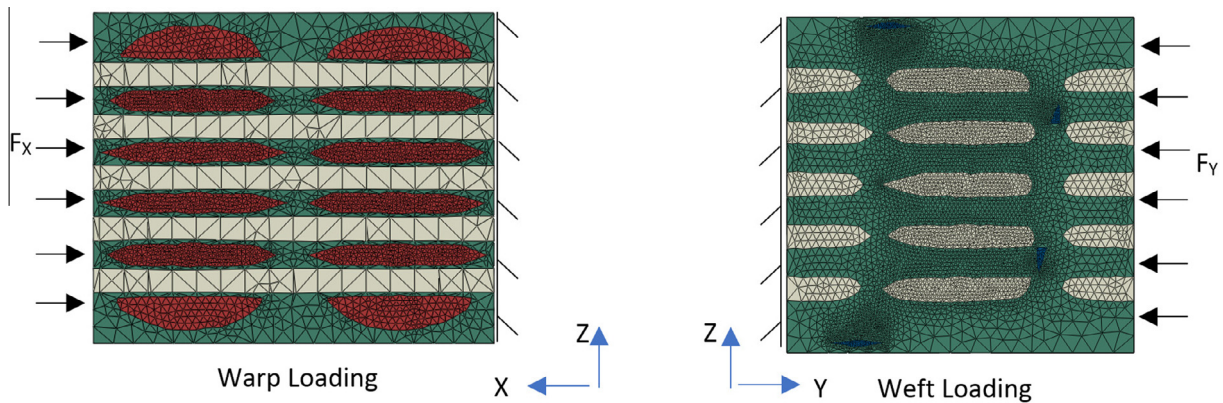


Fig. 13. Description of boundary conditions.

Fig. 13 shows boundary conditions used for weft and warp loading. The face used for load application is allowed to move only in the direction of load application. The face opposite of loading face is restricted for all degrees of freedom. All other faces are unconstrained.

**4. Results**

The fully built model was run using three different analysis types to understand the response and see what information can be captured. First it was run using a quasi-static analysis to calculate the effective Young’s modulus of the material. Then the RUC

was subjected to linear buckling in an Eigenvalue analysis. Finally a Riks simulation was used to look at the onset and progression of damage in the material to determine the fully non-linear curve. Since the model creation approach inherently captures the imperfections, no seeded points are needed.

*4.1. Determination of the elastic modulus of the RUC*

A linear elastic quasi-static analysis was run to determine the effective modulus in the two orthogonal orientations of the material to compare to the idealized geometry RUC. Table 5 shows a comparison of the elastic moduli in both directions for different computational approaches and experimental results. The DE

**Table 5**  
Comparison of elastic moduli.

	Elastic modulus in warp direction (GPa)	Elastic modulus in weft direction (GPa)
Ideal Geometry model [8]	22.68	23.99
Experimental results [8]	21.46	24.55
DE Geometry model	20.27	22.53

geometry shows a 5–8% lower modulus as compared to experimental results.

#### 4.2. Eigenvalue analysis for buckling load estimation

The buckling response of the RUC was simulated by running an eigenvalue analysis. This method is often used in idealized geometry models to get the results for buckling modes and corresponding shapes. This information is further used to seed the imperfection in the RUC. The eigenvalue analysis is a linear buckling simulation, which tends to over predict the actual critical load. However, it is a useful method to get a quick estimate and predict what the buckling shape will look like. This can be helpful to estimate the location of the kink band in a compressive response. Fig. 14 shows first linear buckling mode shapes of the RUC observed in warp and weft directions. Tows in other direction and matrix are not shown since they do not exhibit prominent mode shapes. The corresponding critical load values for entire RUC are reported in Table 6.

The difference between the mode shapes for warp and weft tows is due to the specific structure of the RUC. For example, each warp tow of the RUC has 2 weft tows above and below causing higher resistance to deformation in the region closer to weft tows. Hence at the center, the warp tows deform significantly due to the absence of weft tows. Similarly, the weft tows experience higher deformation between the center and edge of the tow causing dominant deformation in that area while the center is almost unchanged. The Z-fiber tows do not contribute directly to the buckling mode shapes however it is evident that the maximum strain is present at the location where the Z-fiber tow binding action introduces more imperfections and less reinforcement resulting in lower eigenvalue.

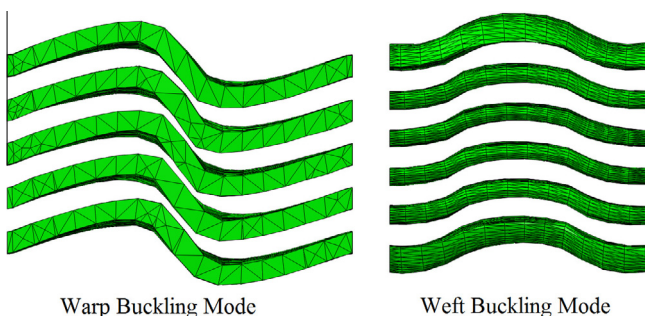


**Fig. 14.** Mode shapes in linear buckling.

**Table 6**  
Critical buckling load based on eigenvalue analysis.

	Critical Buckling Load (kPa)
Warp Tow	1.813
Weft Tow	1.786

#### 4.3. Riks analysis

A Riks analysis was run on the RUC to determine the kink band failure mode in the material. A Riks analysis is essential because it considers structural instability arising from imperfections in the geometry. These imperfections play a major role in the formation of kink bands. Fig. 15 shows the comparison of results along with experimental and ideal geometry simulation results reported in [8] for loading in the weft direction. Riks analysis was also repeated for loading in warp direction (not shown in the figure). While the model is below 1% effective strain, the model behaves in a linear elastic manner. A slight deviation from linearity is noticed at about 1% strain, and this is the onset of the kink band formation from the plasticity in the matrix. The difference in the slopes of different results can be attributed to the differences in volume fractions leading to difference in moduli as reported earlier in Table 5. The critical stress values are compared for each scenario in Table 7. The DE approach can predict the compressive strength of the RUC within 8% accuracy, while an ideal model with an assumed 5% imperfection over predicts the critical stress by about 14%.

With the idealized geometry approach used earlier [8], the nature and extent of imperfections are unknown if the X-ray CT images are not available. Hence, the simulations are rerun by assuming the imperfection shape (such as mode I, mode II etc. obtained from eigenvalue buckling) and the value of imperfection (% deviation from ideal geometry). The analysis is repeated by changing these two artificial imperfection parameters until the results compare well with the experiments [8,9]. This redundant iterative procedure is eliminated by using the DE approach.

Fig. 16 shows a comparison of artificial imperfections in the idealized geometry model versus inherent imperfections in the DE model. Each tow in the DE geometry has its own unique woven signature. For the purpose of comparison, the weft tow at the

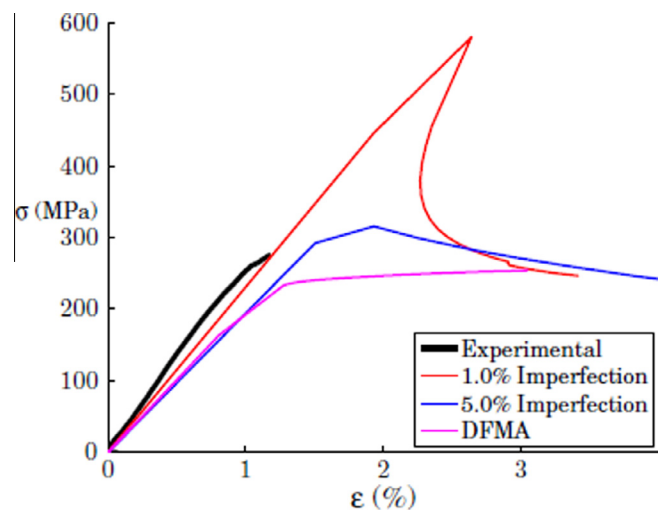


**Fig. 15.** Effective stress–strain plot comparison [8].

**Table 7**  
Effect of imperfection on critical stress based on Riks analysis.

Type of Analysis Model	Critical Stress (MPa)
Experimental [8]	280
Digital Element Approach	260
Ideal Geometry with 1% mode I type imperfection [8]	580
Ideal Geometry with 5% mode I type imperfection [8]	320

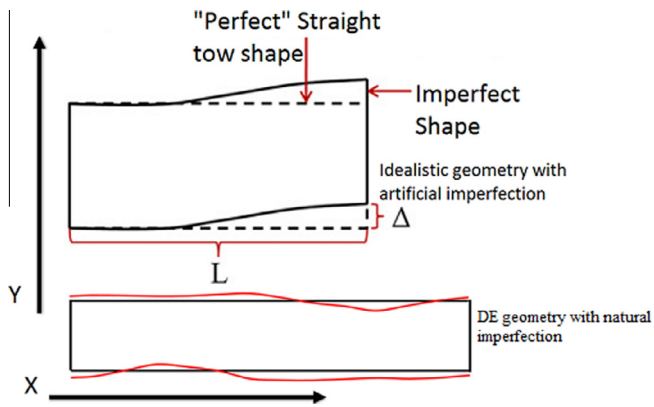


Fig. 16. Artificial imperfection [8] vs inherent imperfection.

center of the RUC is considered. The DE geometry shows natural deviations in the width in top right and bottom left portion of the weft tow in Fig. 16. These deviations are due to Z-fiber tows. For the idealized geometry, it remains straight resulting in a rectangle. For the DE model, the average centerline imperfection is less than 0.1% while the average boundary imperfection is around 0.5%. The maximum imperfection is around 1.6%. Similar trends are observed in the warp tows. However, for the idealized geometry RUC, nature of imperfection, its value and its location need to be approximated. These approximations need to be accompanied by iterative analysis till the response correlates with experimentally observed response. Thus, it required an unrealistic artificial imperfection of 5% based on the failure mode it was seeded it with.

This comparison highlights the benefit of the DE approach compared to an idealized geometry approach as well as comprehensive, realistic geometry approach mentioned in [15]. The DE approach for model creation inherently considers the imperfections and deviations of the tows. This approach eliminates the need to carry out an iterative analysis to validate the assumptions of imperfections as is required with idealized geometry. Additionally, it does not require expensive X-ray CT images for model creation as required with a comprehensive realistic geometry approach. Since the DE approach only needs the overall material parameters, the computational analysis can be performed without actually manufacturing the specimen. Thus, the DE approach results in tremendous savings in model creation and computation time and captures the buckling of tows in an accurate manner.

#### 4.3.1. Effect of yield ratio on Riks analysis

The yield ratio is a factor used in the model to scale the response in any material direction (1, 2 or 3) to the response of pure matrix material. The response of a composite in the transverse direction (2 and 3) is dictated by the matrix properties. Hence the yield ratio in these directions is close to unity. In the axial direction, the composite exhibits very limited plastic response and thus the yield ratio in the axial direction must be high. Based on experimental results of pure matrix material, the yield ratio is varied between 7 and 20 to observe the effects of varying levels of plasticity. Fig. 17 shows the evolution of deformed shape when yield ratio is 7. While the plot correctly shows the elastic loading region, corresponding von mises stress contours do not show a distinct kink band formation. Previous research has shown that a larger number of RUCs are often needed to show the distinct kink band formation [8]. Fig. 18 shows the effect of different values of axial yield ratio (R1) on the effective stress – strain response of loading in weft direction. Corresponding von mises stress contours are plotted at maximum stress values.

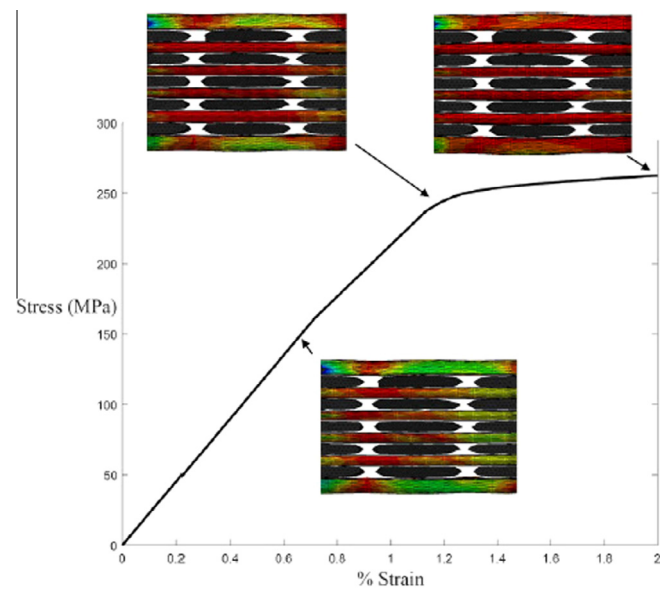


Fig. 17. Evolution of deformed shape in weft loading.

Increasing the yield ratio increases the yield point of the composite without changing the elastic modulus. As observed from the deformed shape of the tows, a higher yield ratio causes higher stress levels in the tows but the overall deformed shape of the tows is almost unchanged. Based on the stress contour and deformed shape, the results do not appear to capture kink band formation. Additionally, the simulations show that the experimentally observed sudden load drop at buckling can only be predicted for ratios higher than 15. However, at this yield ratio, the critical load is over predicted as the instability of the tow will take over before the plasticity and failure can become dominant. Therefore, distinct kink bands never form. The current tow material model does not allow for varying amounts of plasticity in the different directions. A user defined material would need to be created to capture this type of variation.

#### 4.3.2. Effect of multiple RUCs on the Riks analysis

A single RUC is not effective at capturing the kink band formation as reported in section 4.3.1. A multiple RUC model has more imperfections and longer tows, allowing for kink bands to form more readily as they will not run into the model boundaries. A 4RUC model (2 in each direction) was created for the purpose of this analysis. The overall arrangement pattern of fiber tows inside any RUC of the specimen is identical. However, every RUC has unique imperfections. Hence this model is created by actually constructing the larger RUC rather than simply duplicating the geometry in each direction. The loading and boundary conditions are identical to the previous single RUC model. The mesh refinement and material properties from the previous model are also used for this analysis. Table 8 compares the single RUC and 4RUC mesh with approximate run time where a 4 core cluster was used to execute the jobs.

Fig. 19 shows the comparison of experimental observations of kink bands with that of the computational results for the 4RUC model showing von mises stress. 4RUC model effectively captures the formation of kink band at about  $45^\circ$ . This kink band is observed at peak stress value when  $R1 = 15$ . Fig. 20 shows the comparison of the effective stress – strain response of a single RUC with the 4RUC model. The 4RUC model shows a drop in peak load of about 12% as compared to the single RUC model. This difference highlights the effect of the size of the model on peak load for buckling failure.

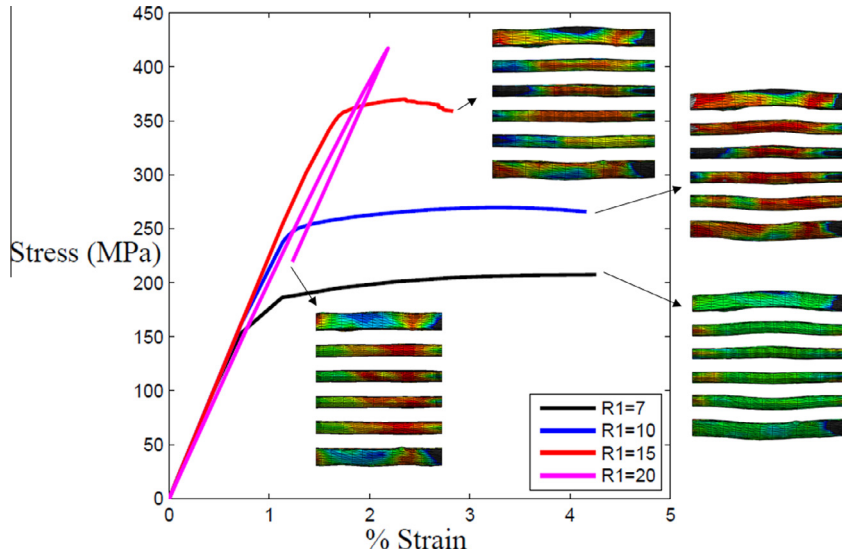


Fig. 18. Effect of yield ratio on the response of compression loading in weft direction.

Table 8  
Mesh and analysis comparison for single and multiple RUC model.

	1 RUC	4 RUC
No. of Nodes	64,398	104,907
No. of Elements	339,960	605,026
Analysis Run Time (Hours)	2.3	3.6

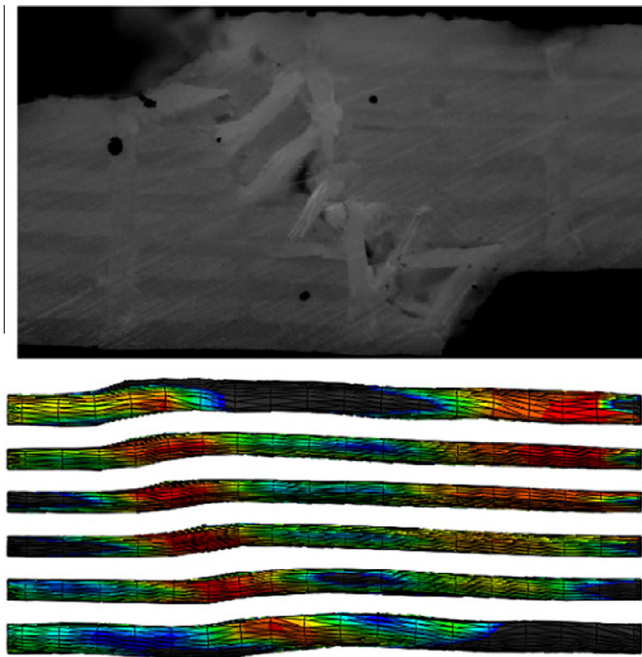


Fig. 19. Comparison of kink band formation [8].

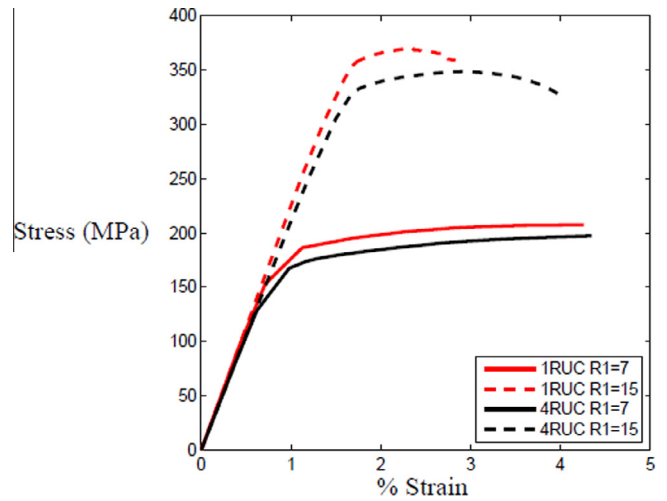


Fig. 20. Effect of multiple RUC on the response of compression loading in weft direction.

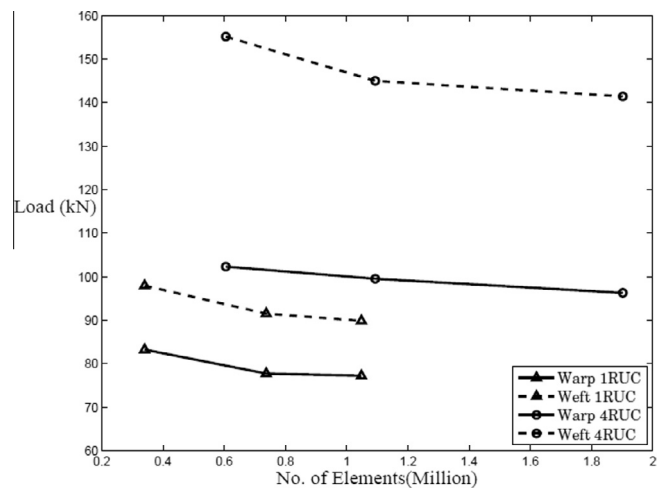


Fig. 21. Effect of mesh refinement on critical buckling load.

4.3.3. Effect of mesh density on the critical buckling load

The effect of the number of elements on eigenvalues was evaluated for models with varying mesh density. As shown in Fig. 21, the difference was found to be less than 7% for three times the number of elements. This shows that the mesh refinement used in this analysis is sufficient.

**5. Conclusion**

The digital element approach using DFMA™ has been successfully implemented for modeling the imperfections and deviations in the fiber tow geometry. This method was used to analyze quasi-static buckling of 3D woven composites. A Riks analysis of this model accurately predicts critical buckling loads and the onset of kinking without seeding the model with artificial imperfections. The iterative procedure for an idealized geometry model required to estimate the imperfection in the actual specimen is eliminated. This approach also gives useful results to predict kink band formation in the specimen. As with previous studies, it was shown that the number of RUCs modeled affects the results. However, this method lends itself to multiple RUCs as we can digitally weave a larger portion and capture more unique geometry rather than just putting individual RUCs together as is typically done with an idealized geometry model. The accuracy of results increases as the model size approaches the specimen size used in conducting experiments.

**Acknowledgements**

The authors would like to thank Army Research Lab for their continued input and direction.

**Appendix A**

*A.1. RUC model creation in fabric mechanics DFMA™*

It is recommended to enter all the properties in SI units for easier transition and compatibility with FE analysis software.

*A.1.1. Define yarn properties*

Total yarn types entered as 3 corresponding to weft, warp and z-fiber. Cross sectional area, elastic modulus in transverse and axial directions, strength and fiber density are entered for each yarn type. The number of actual fibers per yarn (typically in the order

of thousands) is also entered for each yarn type. The bending stiffness flag can be neglected and hence entered as 0.

*A.1.2. Unit cell topology*

The 3D woven type is chosen. Generally, it is suggested to create at least 4 RUCs in a model rather than a single RUC. Hence, length and width parameters will be double than single RUC. For each of the warp sections, the total number of tows (warps + Z-Fibers) is defined and then the arrangement of the tows needs to be defined in tabular form (Fig. A1).

*A.1.3. Digital element mesh and remesh*

This provides 3 controls viz. Fibering, Elementing and Scaling. Scaling is applied only in z direction to reduce the thickness and achieve higher volume fraction (Table A1).

*A.1.4. Periodic geometry and relaxation*

These parameters provide the controls for an iterative procedure to achieve next step geometry. For most of the parameters, help guidelines in the software are followed. Some differences are mentioned next. Boundary conditions should be imposed so as to restrict the displacement of fibers out of the RUC. Thus warps and Z-Fibers are restricted in X direction while wefts are restricted in Y direction. Sometimes, removing the boundary conditions in the initial steps allows the fibers to easily acquire realistic shape. Target tension is defined on yarn types and varied between 1e-4 to 0.2. Relaxation parameters contain many sub parameters. Solution time step is varied from 900 to 5000. Gap factor is set at 0.3 to restrict yarn interpenetration.

*A.1.5. Solid yarn model*

The yarn model parameters control the mesh resolution of the geometry. The ratio d/R controls the length of the element and is set at 0.5 for Z-Fibers and 1.2 for warp and wefts. Number of nodes per section is adjusted by setting the parameter 'n' to 32 for all types of tows. Rs/r and Tol/r control the perimeter geometry and they are set to 10 and 0.1 respectively.

Input weft pattern and warp sections:

Cell Length:       Cell Width:

Weft Layers:       Weft Columns:       Warp Sections:

Input warp numbers per warp Section:

	Warp Numbers
<b>Section 1</b>	5
<b>Section 2</b>	1
<b>Section 3</b>	1
<b>Section 4</b>	5
<b>Section 5</b>	1
<b>Section 6</b>	1
<b>Section 7</b>	5
<b>Section 8</b>	1
<b>Section 9</b>	1
<b>Section 10</b>	5
<b>Section 11</b>	1
<b>Section 12</b>	1

Fig. A1. Overall topology input parameters.

**Table A1**  
Warp section arrangement in tabular form.

	1	2	3	4	Yarn Type
<i>Warp section 1</i>					
#1	1	1	1	1	2
#2	2	2	2	2	2
#3	3	3	3	3	2
#4	4	4	4	4	2
#5	5	5	5	5	2
<i>Warp section 2</i>					
#1	6	0	0	6	3
<i>Warp section 3</i>					
#1	0	6	6	0	3
<i>Warp section 4</i>					
#1	1	1	1	1	2
#2	2	2	2	2	2
#3	3	3	3	3	2
#4	4	4	4	4	2
#5	5	5	5	5	2
<i>Warp section 5</i>					
#1	6	6	0	0	3
<i>Warp section 6</i>					
#1	0	0	6	6	3
<i>Warp section 7</i>					
#1	1	1	1	1	2
#2	2	2	2	2	2
#3	3	3	3	3	2
#4	4	4	4	4	2
#5	5	5	5	5	2
<i>Warp section 8</i>					
#1	6	0	0	6	3
<i>Warp section 9</i>					
#1	0	6	6	0	3
<i>Warp section 10</i>					
#1	1	1	1	1	2
#2	2	2	2	2	2
#3	3	3	3	3	2
#4	4	4	4	4	2
#5	5	5	5	5	2
<i>Warp section 11</i>					
#1	6	6	0	0	3
<i>Warp section 12</i>					
#1	0	0	6	6	3

## References

- [1] Cox B, Dadkhah M, Inman R, Morris W, Zupon J. Mechanisms of compressive failure in 3D-composites. *Acta Metall Mater* 1992;40(12):3285–98.
- [2] Cox B. Delamination and buckling in 3D composites. *J Compos Mater* 1994;28(12):1114–26.
- [3] Fleck N, Jelf P, Curtis P. Compressive failure of laminated and woven composites. *J Compos Tech Res* 1995;17(3):212–20.
- [4] Cox B, Dadkhah M, Morris W, Flintoff J. Failure mechanisms of 3D woven composites in tension, compression, and bending. *Acta Metall Mater* 1994;42(12):3967–84.
- [5] Stig F, Hallstrom S. Assessment of the mechanical properties of a new 3D woven fibre composite material. *Compos Sci Technol* 2009;69(11–12):1686–92.
- [6] Tan P, Tong L, Steven G. Modeling approaches for 3D orthogonal woven composites. *J Reinf Plast Compos* 1998;17(6):545–77.
- [7] Stig F, Hallstrom S. A modelling framework for composites containing 3D reinforcement. *Compos Struct* 2012;94(9):2895–901.
- [8] Pankow M, Waas A, Yen C. Modeling the response of 3D textile composites under compressive loads to predict compressive strength. *Comput Mater Cont* 2012;32(2):81–106.
- [9] Song S, Waas A, Shahwan K, Faruque O, Xiao X. Compression response, strength and post-peak response of an axial fiber reinforce tow. *Int J Mech Sci* 2009;51:491–9.
- [10] Isart N, El Said B, Ivanov D, Hallett S, Mayugo J, Blanco N. Internal geometric modelling of 3D woven composites: a comparison between different approaches. *Compos Struct* 2015;132:1219–30.
- [11] Green S, Long A, El Said B, Hallett S. Numerical modelling of 3D woven preform deformations. *Compos Struct* 2014;108:747–56.
- [12] Yushmanov S, Bogdanovich A. Fiber waviness in textile composites and its stochastic modeling. *Mech Compos Mater* 2000;36(4):297–318.
- [13] Lomov S. Composite reinforcements for optimum performance. In: Boisse P, editor. Woodhead Publishing; 2011. p. 200–38.
- [14] Long A, Brown L. Composite reinforcements for optimum performance. In: Boisse P, editor. Woodhead Publishing; 2011. p. 239–64.
- [15] Vanerschot A, Cox B, Lomov S, Vandepitte D. Experimentally validated stochastic geometry description for textile composite reinforcements. *Compos Sci Technol* 2016;122:122–9.
- [16] Wang Y, Sun X. Digital-element simulation of textile processes. *Compos Sci Technol* 2001;61(2):311–9.
- [17] Green S, Matveev M, Long A, Ivanov D, Hallett S. Mechanical modelling of 3D woven composites considering realistic unit cell geometry. *Compos Struct* 2014;118:284–93.
- [18] Huang L, Wang Y, Miao Y, Swenson D, Ma Y, Yen C. Dynamic relaxation approach with periodic boundary conditions in determining the 3-D woven textile micro-geometry. *Compos Struct* 2013;106:417–25.
- [19] Drach A, Drach B, Tsukrov I. Processing of fiber architecture data for finite element modeling of 3D woven composites. *Adv Eng Softw* 2014;72:18–27.
- [20] Pankow M, Waas A, Yen C. Modeling the response, strength and degradation of 3D woven composites subjected to high rate loading. *Compos Struct* 2012;94(3):1590–604.
- [21] Herakovitch C. Mechanics of fibrous composites. New York: McGraw-Hill; 1998.

- [22] Pankow M, Waas A, Yen C, Ghiorse S. A new lamination theory for layered textile composites that account for manufacturing induced effects. *Compos A Appl Sci Manuf* 2009;40(12):1991–2003.
- [23] Heinrich C, Aldridge M, Wineman AS, Kieffer J, Wass AM, Shahwan K. The influence of the representative volume element (RVE) size on the homogenized response of cured fiber composites. *Model Simul Mater Sci Eng* 2012;20(7).
- [24] Zhang D, Waas A, Pankow M, Yen C, Ghiorse S. Flexural behavior of a layer-to-layer orthogonal interlocked three-dimensional textile composite. *J Eng Mater Technol* 2012;134(3).
- [25] Zhou G, Sun X, Wang Y. Multi-chain digital element analysis in textile mechanics. *Compos Sci Technol* 2004;64(2):239–44.
- [26] C. Yen, in *American Society of Composites*, Dayton, 2010.